European Organisation for Astronomical Research in the Southern Hemisphere
Observing Programmes Office • Karl-Schwarzschild-Strasse 2 • D-85748 Garching bei München • email: opo@eso.org • Tel: +49 89 3200 6473

Cycle: P112
Type: Large
Status: Valid
Printed: 09 Aug 2023

APPLICATION FOR OBSERVING TIME 112.262L

IMPORTANT NOTICE

By submitting this proposal, the PI takes full responsibility for the content of the proposal, in particular with regard to the names of CoIs and the agreement to act according to the ESO policy and regulations, should observing time be granted.

The cosmic Ecosystem of the first QSOs and Galaxies: a MUSE/XSHOOTER/JWST/ALMA Legacy Survey

ABSTRACT

QSOs at z~6 are among the brightest sources in the Universe and are unparalleled tools to investigate the first billion years of Cosmic History. The high density of the infant Universe leads to vigorous episodes of galaxy formation and rapid evolution, which we are only now starting to unveil. With this large program we propose to take the next leap forward in our view of the build up of the first galaxies through a deep (4 hours per target) legacy survey of a sample of 40 bright (M_1450<-26mag) QSOs at z>5.8 already observed with ALMA and XSHOOTER. MUSE will provide a spectroscopy survey along the entire QSO light cones, resulting in the detection of the Lyα emission in ~100 galaxies at 4.0<z<6.6 (the redshift of interest for this program) in a volume of 2.4x10^5 cMpc^3, including 20-30 galaxies physically associated to the central QSOs. Additionally, the proposed observations will be sensitive enough to expose, with unprecedented detail, the diffuse ionized gas in the QSO's immediate environment via its Lyα emission. The unique synergy of three of the most powerful ESO instruments will produce a transformative data-set to address many outstanding questions of early galaxy formation: i) Which environment led to rapid formation of massive black holes in such short cosmic times? ii) How did the first galaxies pollute the gas at intergalactic scales? iii) Which galaxies are responsible for the reionization?

More in general, owing to high-quality spectroscopy from the ground, the proposed MUSE observations will provide the most complete view of the first stages of the co-evolution of galaxies with their close environment to date. In addition, JWST is offering an exceptional complement to the proposed observations, by providing exquisite follow-up of the rest-frame optical emission lines for 16 of the proposed targets. The unparalleled combination of MUSE, XSHOOTER, ALMA, and JWST data will be a long lasting legacy, placing the ESO community in a privileged position to undertake the first systematic study of the ISM metallicity (traced by, e.g., oxygen lines), star formation rates (traced by hydrogen recombination lines), ISM properties (traced by ALMA observations), and CGM physical content (traced by metal lines in absorption) and to finally paint a coherent picture of the link between galaxy and halo gas properties in what are poised to become the best studied fields for the CGM-galaxy co-evolution in the first billion years of cosmic history. Setting the stage for further exploration of the epoch of reionization using the E-ELT.

SCIENTIFIC KEYWORDS

cosmology: early universe, cosmology: dark ages, reionization, first stars, galaxies: high-redshift, galaxies: quasars, galaxies: evolution

RUNS

Run	Period	Instrument	Tel. Setup	Constraints	Mode	Type	Propr. Time	Time Constr.	Req. Time
112.262L.001 • Run 1	112	MUSE	UT4	FLI: 70% • Turb.: 85% • pwv: 30.0mm • Sky: Variable, thin cirrus	SM	Normal	12m	×	81h00m
112.262L.002 • Run 2	113	MUSE	UT4	FLI: 70% • Turb.: 85% • pwv: 30.0mm • Sky: Variable, thin cirrus	SM	Normal	12m	×	66h00m

AWARDED AND FUTURE TIME REQUESTS

Time already awarded to this project

- none -

Future time requests to complete this project

- none -

Special Remarks

The complete sample consists of 40 bright [J(AB)<20.5mag] QSOs at 5.8<z<6.6. Five of which have already been observed with MUSE at a depth comparable with the proposed observations (i.e., ~5 hours on target) and thus not included in this proposal. Eighteen of the selected QSOs are part of the MUSE filler program presented in Farina et al. (2019). This consists of short integrations (~45min per target) collected in poor seeing conditions (Turb.=100%) that do not fulfill the quality necessary to achieve the ambitious goals of our program.

All selected QSOs have been already observed with XSHOOTER and ALMA. Thus, the main properties of their central black holes (masses and accretion rates) and of their host galaxies (dust and dynamical masses and star formation rates) have already been secured (e.g., Farina et al. 2022, Venemans et al. 2020) . In addition, XSHOOTER spectroscopy revealed ~300 foreground strong absorption systems in the redshift range 4<z<6 (Davies et al. 2023). Our MUSE observations will be able to detect galaxies slightly fainter than L* located within 200 kpc from these high-

redshift absorbers. Finally, 16 of the selected QSOs are also target of JWST GO and GTO programs which will provide complementary information on the rest-frame optical properties of the central QSOs and of 5.3<z<6.9 galaxies in their fileds (e.g., Eilers et al. 2022, Kashino et al. 2022).

Scientific Rationale: The Rise of the First Massive Galaxies

One of the ultimate frontiers in astronomy is to explore the so-called "cosmic dawn", when the first stars, galaxies, and AGNs formed and marked the beginning of the last phase transition of the Universe: the epoch of reionization. This watershed epoch inaugurated the era in which the cosmic gas cycle gained a dominant role in the formation and evolution of galaxies. Substantial theoretical efforts are currently dedicated to exploring these early stages of galaxy formation (e.g., Kannan et al. 2022, Habouzit et al. 2022, Costa et al. 2022). The emerging picture is that the first galaxies are strongly entangled with their cosmic ecosystems. On one hand, the close environment of galaxies regulates their growth via interactions, mergers, and gas inflows. On the other hand, ionizing photons and metal enriched gas escaping the newly formed galaxies influence and pollute the surrounding medium, ultimately affecting the formation of the second generation of stars. The goal of this Large Program is to provide a solid observational ground to test the onset of this connection in the first billion years of cosmic history by collecting deep (4 hours on source) MUSE integrations of a sample of 40 bright ($M_{1450}<-26$ mag) QSOs at $5.8<z<6.6$ (Fig. 1). By complementing archival high-quality (S/N$\gtrsim$10 per resolution element) XSHOOTER spectra (e.g., D'Odorico et al. 2022) and high-resolution ($<0.15''$) ALMA maps of the host galaxies (e.g., Venemans et al. 2021), this survey will provide the community with a powerful redshift survey along the QSO light-cones thus delivering **the most comprehensive study of the IGM, CGM, and galactic environment at the early cosmic times**.

ESO and the Golden Age for High-z QSO Studies: The last years has seen a surge in studies of galaxies at early cosmic times, mainly driven by the launch of JWST (Curti et al. 2022, Fujimoto et al. 2023). As the most luminous long-lived objects in the Universe (typically >1000 times brighter than *normal* galaxies at the same redshifts), QSOs are the workhorses to investigate structure formation at early cosmic times. Indeed, as the number of known $z>6$ QSOs steadily increases (Fan et al. 2022), questions about the formation and evolution of the first galaxies can be tackled with a systematic and homogeneous approach. This proposal builds on a large effort by the ESO community to collect high-quality XSHOOTER and ALMA observations of a statistical sample of $z>6$ QSOs. This dataset has already revolutionized our view of galaxies at the epoch of reionization, revealing that: *(i)* SMBHs with masses exceeding 10^9 $M_\odot$ are present less than a billion years after the Big-Bang (Farina et al. 2022); *(ii)* the QSO host galaxies are building their stellar mass at prodigious rates (SFR>100 $M_\odot$ yr^{-1}) but are still under-massive with respect to their SMBHs, if compared with samples at lower redshifts (Venemans et al. 2020, Neeleman et al. 2021); *(iii)* the IGM rapidly converts, with large fluctuations, its status from mostly ionized to mostly neutral in the redshift range $z\sim$6-7 (Bosman et al. 2022); *(iv)* the CGM of reionization-era galaxies is highly chemically enriched, suggesting that a substantial fraction of baryons has already been recycled from previous generations of star forming winds while their dark matter halos were still assembling (D'Odorico et al. 2022, Davies et al. 2023a). Many puzzles regarding the population of $z>6$ galaxies, however, still remain unsolved: *How do the first galaxies accrete their gas? Which environments enable the rapid formation of the first SMBHs? What is the escape fraction of UV and Lyα photons produced by the first bursts of star formation? How and how fast do galaxies pollute their environs with metals?* We argue that an answer to these long–standing questions requires a definitive homogeneous spectroscopic survey of a statistical sample of high-z QSOs.

Sample size and Required depth: This experiment aims at detecting $\gtrsim$100 Lyα-emitters (LAEs) at $4<z<6.6$ and extended Lyα nebulae in the field of 40 high-z QSOs, in order to: **a)** Measure the clustering of LAEs around a sizable sample of high-z QSOs, finally constraining the environment where the earliest SMBHs are able to form; **b)** Image the circum-galactic Lyα emission around the first QSOs on scales of tens of kilo-parsecs, providing insights on the gas reservoirs feeding the first massive galaxies; **c)** Assemble a large statistical sample of foreground galaxies linked to XSHOOTER detected absorbers and Lyα transmission spikes in order to *(i)* probe the metal enrichment and ionization state of the CGM of $4<z<6.6$ galaxies and *(ii)* constrain the galaxy contribution to reionization via direct measurements of their ionizing photon escape. Our observing strategy is tailored to tackle the aforementioned points. The exposure time is scaled to detect galaxies 2$\times$ fainter than the characteristic luminosity of LAEs at $z\sim$6 [i.e., with L(Lyα)$\gtrsim 9\times10^{42}$ erg s^{-1}] to maximize the number of galaxies detected in a single pointing. Indeed, the steep bright side and the much shallower faint end of the luminosity function (Santos et al. 2016) ensures that we will detect (on average) 0.5 bright LAEs per field at the QSO redshift (extrapolating from $z\sim$4 clustering results), yielding a solid detection of the small scale QSO-galaxy clustering ($\gtrsim 5\sigma$, Fig. 4). At the same time, we will constrain the galaxy-IGM cross correlation at $\gtrsim 8\sigma$ (Fig. 5) and [based on our survey depth and the detection rate (1/4) of absorber host galaxies at similar flux limits, Díaz et al. 2021] uncover $\sim$80 galaxy-absorber pairs from the $\sim$300 absorbers identified in XSHOOTER spectra (Davies et al. 2023b, Fig. 3). Two alternative scenarios can be considered to obtain a similar precision in the QSO-galaxy clustering measurement: *a)* Shallower exposures of 2 hours per target, which require a 4$\times$ larger sample of QSOs, resulting in a request of 1.6$\times$ more telescope time. *b)* Deeper integrations of 10 hours per target, which will increase the number of LAEs detected in each field only by a factor of 1.6$\times$, effectively resulting in a factor 1.3$\times$ increase in telescope time. While this latter option could be viable, the cosmic variance would plague the results obtained from a smaller sample of $\sim$15-20 QSOs, reducing the significance of our results by a factor of $\gtrsim$2 (e.g., only one of the three $z\sim$6 QSOs observed with MUSE by Meyer et al. 2022 shows the presence of a LAE's overdensity, Fig. 4). Thus, we conclude that targeting a luminosity limited sample (which has the least selection bias) of 40 QSOs with 4 hours integrations is the best approach.

MUSE and the Missing Link: Galaxies and their Close Environment

To date, 28 bright ($M_{1450}<-26$ mag) $z>5.8$ QSOs have been observed with MUSE, however, only 10 of these have integrations longer than 1 hour. The analysis of these *shallow* fields is already showcasing the unique capabilities of MUSE in dissecting the immediate environment of galaxies at the reionization epoch (e.g., Farina et al. 2019). However, the combination of the deepest MUSE integrations and sensitive ALMA and XSHOOTER observations represents a change of gears in our understanding of the first galaxies and QSOs. In addition, JWST offers an exceptional complement to the proposed observations, by providing exquisite follow-up (via IFU and slitless grism observations) of the rest-frame optical emission lines. In the following, we will detail the immediate goals of our program which will quadruple the number of sightlines with high quality MUSE, XSHOOTER, and ALMA data and includes 16 of the QSOs selected as target of JWST GTO and GO programs.

1) Detect the Ionized Gas Around z∼6 QSOs: The mere presence of 10^9 $M_\odot$ SMBHs at $z\sim6$ is challenging our understanding of SMBH and galaxy formation. The growth time for black holes is, indeed, relatively short, with an e-folding time scale of 45 Myr when accreting at Eddington (Volonteri & Rees 2005). Thus, there is barely enough time for a 100 $M_\odot$ black hole seed to grow to 10^9 $M_\odot$ in less than 1 Gyr (Inayoshi et al. 2020). To sustain such a rapid growth, the first QSOs need a continuous replenishment of fresh fuel provided by filamentary streams of T=10^4-10^5K gas from the IGM. When illuminated by the bright QSO radiation, this fundamental ingredient of early galaxy formation can be directly mapped as an extended "fuzz" of fluorescent $\mathrm{Ly}\alpha$ emission (Haiman & Rees 2001). In the last years, MUSE showed that detecting these nebulae around $z\sim6$ QSO hosts is indeed possible (Farina et al. 2019, Drake et al. 2019). However, these preliminary results (mainly based on 45 min integration) only expose the brightest knots of the extended $\mathrm{Ly}\alpha$ emission. Dedicated cosmological, radiation–hydrodynamic simulations of $z>6$ QSO host halos (Costa et al. 2022) shows that observations a factor 2-3× deeper than those available (i.e., reaching 5σ limits of $\sim10^{-18}$ erg s^{-1} cm^{-2} arcsec^{-2}) are necessary to constrain the morphology and shape of the $\mathrm{Ly}\alpha$ line and thus infer the physical mechanism of the emission (and, ultimately, derive the properties of the gas, Fig. 2). These simulations also exposed that the properties of the gas reservoirs are, indeed, the result of many relevant processes in early structure formation (including metal and gas enrichment due to galaxy scale outflows, possibly driven by the SMBH activity). In particular, AGN-driven outflows, besides modifying the temperature and density of the gas in the halo, cause a dramatic drop in the H I and dust optical depths in the host galaxy, facilitating the escape of $\mathrm{Ly}\alpha$ photons from the galactic nucleus. Thus establishing a strong causal connection between AGN feedback and $\mathrm{Ly}\alpha$ nebulae. With this proposal we will be able to provide firm observational constraints on this prediction by linking intrinsic properties of the halos with SMBH-driven winds identified in XSHOOTER spectra (10 of the selected QSOs are classified as BAL, Bischetti et al. 2022), with molecular outflows traced by the OH 119μm doublet absorption in ALMA data (Butler et al. 2023), and with warm outflows identified in maps of the [O III] lines accessible via JWST. We will thus be able to **constrain the physical properties of the gas surrounding massive galaxies 1 Gyr after the Big Bang with unprecedented details**.

2) Probe the Galactic Environment of the First QSOs: A fundamental result of the ΛCDM structure formation paradigm is that the clustering of a population can be directly related to their host dark halo masses (Mo & White 2002). The analysis of the QSO-QSO clustering at $z\sim2$ shows that bright QSOs are biased tracers of massive dark matter haloes with $M_{DM}>10^{12.5}M_\odot$ (White et al. 2012). Several studies point towards a strengthening of the clustering from $z\sim2$ to $z\sim4$ (Shen et al. 2007, Eftekharzadeh et al. 2015), the highest redshift for which it has been measured. Unfortunately, the extremely low space density of $z>6$ QSOs precludes the possibility of measuring their auto-correlation function [$\xi_{\mathrm{QQ}}(r)$]. A complementary approach to determine QSO host halo masses is to measure the clustering of galaxies around them. If quasars and galaxies trace the same dark matter overdensities, the quasar-galaxy cross-correlation [$\xi_{\mathrm{QG}}(r)$], can be uniquely predicted given the respective auto-correlation of QSOs and galaxies [$\xi_{\mathrm{GG}}(r)$]. While theoretical models generally predict that to form 10^9 $M_\odot$ SMBHs at $z\sim6$, luminous high-z QSOs must reside in the rarest peaks of the initial distribution of density fluctuations and are thus hosted by the most massive dark matter halos (Volonteri 2012). Investigations of the Lyman-Break galaxies and LAEs clustering around $z\sim6$ QSOs resulted inconclusive: while some studies reported indications of overdensities (Mignoli et al. 2020), others revealed number counts consistent with (or even lower than) the blank fields (Mazzucchelli et al. 2017; Goto et al. 2017). These studies, however, are based on one-few targets each and a detailed, quantitative interpretation is hampered by differing methodologies and heterogeneous detection criteria. Meyer et al. (2022) demonstrated the relevance of deep (>3 hours) MUSE integrations to to derive $\xi_{\mathrm{QG}}(r)$ by reporting the detection of LAEs around three $6<z<6.6$ QSOs. These preliminary findings are suggestive for a dense environment, consistent with a QSO-LAEs cross-correlation length of $r_0^{\mathrm{QG}}\sim10\,h^{-1}$cMpc (Farina et al. 2017) and with independent constraints on the small-scale ($<1\,h^{-1}$cMpc) clustering derived from the two $z>5$ binary QSOs known to date (McGreer et al. 2016, Yue et al. 2021). While these results are intriguing, the large cosmic variance inherent in QSOs environment studies and the small number statistic of the detected LAEs prevent to derive more quantitative conclusions. Here we propose to perform a systematic search of LAEs surrounding a statistical sample of high-z QSOs. With our sample of 40 QSOs, we will be able to detect ∼20-30 LAEs associated with the QSOs, allowing us to infer the QSO-galaxy clustering at $\gtrsim5\sigma$ and thus **place quantitative constraints on the immediate environment where the first QSOs reside** (Fig. 4). We stress that different

type of galaxies have different clustering properties. For instance, ALMA has detected bright [C II]-emitting close companions (< 100 pkcp) around 4 out of 27 fields, implying that dusty star forming galaxies (virtually invisible at UV-wavelengths, Mazzucchelli et al. 2019) are strongly clustered around QSOs (Decarli et al. 2017, Fig. 4). In particular, our sample contains all the z<6.6 QSOs visible from Paranal part of the JWST programs ID#2078 and ID#1243 which target Hβ+[O III] line emitters in the proximity of $z\sim$6-7 QSOs via slitless spectroscopy, thus measuring $\xi_{\rm QG}(r)$ (Kashino et al. 2022). For these targets, the proposed MUSE observations will pinpoint the underlying overdensity with a complementary tracer. Indeed, the Hβ+[O III] emitters are hosted by $\sim10^{12}$M$_\odot$ dark matter halos (Khostovan et al. 2018), while LAEs are hosted by less massive $\sim10^{10-11}$M$_\odot$ ones (Ouchi et al. 2010). Therefore, the comparison of the spatial distribution of LAEs and Hβ+[O III] emitters in QSO vicinity will unveil whether the strong QSO UV radiation affects the formation of different types of galaxies as suggested by some theoretical works (Kashikawa et al. 2007). This will provide valuable insights into the physical processes that trigger QSO activity and will help to explain how the first QSOs are embedded in the structure formation hierarchy.

3) What is the origin of the first metal absorbers: Due to the diffuse nature of the IGM/CGM, with densities $n_{\rm H}$<0.1 cm^{-3}, absorption lines detected against QSOs are the best way to study the distribution, kinematics and chemical properties of gas at the interface between galaxies and the cosmic web, with similar sensitivity at all redshifts. In the last decades, there have been significant efforts in understanding the connection between the CGM probed in absorption and galaxies detected in emission at 2<z<4 (e.g., Rubin et al. 2010, Bielby et al. 2017, Lofthouse et al. 2023). These experiments revealed a complex picture, with a metal-enriched and multiphase CGM, with kinematics consistent with the presence of inflows and outflows inside and near halos (e.g., Turner et al. 2017). On the other hand, the CGM-galaxy connection encompassing the crucial redshift range $z\sim$4-6 is still largely unexplored. Theoretical works predict drastic changes of the CGM while approaching reionization due to the increase in the gas accretion rate, the decrease of the amount of metals, and the changes in the ionization status of the Universe (Finlator et al. 2020). Recently, Davies et al. (2023b) delivered the (to date) largest sample (~ 300) of 4<z<6.3 absorbers detected in high-quality XSHOOTER spectra. This study robustly constrained the quick decrease of C IV cosmic mass density between $z\sim$4.7 and $z\sim$5.8, accompanied by an increase in C II at z>5.2 Davies et al. (2023a). At the same time, the incidence of weak low-ionization absorbers (e.g., Mg II, O I) remains constant or increases (Chen et al. 2017, Becker et al. 2019). These results suggest that reionization indeed plays a significant role in the evolution of C IV at z>5, but that chemical composition of the CGM needs to evolve rapidly at lower redshift. This implies that the enrichment of the CGM was under-way quite early, while the dark matter halos of future galaxies were still assembling. At $z\sim$5-6, however, there is scarcely enough time for a halo to accrete gas into its center, develop a stellar population, deposit feedback into the surroundings, and transport such material far enough back into the halo to produce an appreciable absorption cross section. Alternatively, the CGM could be enriched by elements manufactured in accreted satellites or other in-situ star formation environments before they are incorporated into the galaxy ISM. This would especially be true if early absorbers preferentially occur in rich or highly biased environments where the earliest galaxies would have formed. By combining MUSE data with the z>4 metal absorbers detected with XSHOOTER we will explore these scenarios by undertaking **the first systematic analysis of ions inside the multi-phase CGM of z>4 galaxies** (see Fig. 3), thus probing the ejection of metals, trace the expansion of the metal enriched bubbles, and connect their properties with the "fossil" record seen near galaxies at later cosmic epochs. The combination of deep XSHOOTER and MUSE integrations has already proved to be effective in testing the connection between faint LAEs and the z>4 C IV absorbers (Bielby et al. 2020, Díaz et al. 2021) in the spectrum of QSO J1030+0524. Extrapolation from these pilot studies, we expect to probe ~80 galaxy-absorber z>4. We stress that the proposed MUSE observations will complement the ongoing JWST effort. The redshift range for detecting Hβ+[O III] with JWST slitless spectroscopy is $z\sim$5.3-7, while with our sample we will be able to consistently bridge such study from z=4 (post-reionization) to z=6 (during reionization).

4) How do galaxies contribute to reionization? Understanding cosmic reionization is of prime importance for cosmology. Its timing is now constrained to be in the range 6<z<15 (Planck Collaboration et al. 2018), and a late, rapid, and patchy reionization process down to $z\sim$5.5 (Greig & Mesinger 2017) is supported by a large set of observations such as the Lyα forest opacity (Bosman et al. 2022), the decline of the fraction of LAEs (Pentericci et al. 2018), the number of "dark pixels" in the Lyα forests at z<6 (Zhu et al. 2021), and the damping wing detected in z>7 QSO spectra (Davies et al. 2018). Nonetheless, the properties of the galaxies driving reionization and their relative contributions are less clear. Recent studies suggest that faint galaxies could dominate the ionizing photon budget if their escape fraction of ionizing photons is large ($f_{esc}\gtrsim$0.1, Finkelstein et al. 2019). However, Lyman-continuum photons cannot be directly detected at z>5 due to line blanketing from the foreground IGM. Excess IGM transmission is however expected around bright galaxies, which trace enhanced ionizing background produced by a faint clustered population (Kakiichi et al. 2018, Kashino et al. 2022). The ionizing output of all galaxies down to M$_{\rm UV}\lesssim$-10 mag can therefore be constrained via the cross-correlation of foreground galaxies with the Lyα and Lyβ transmission spikes in QSO spectra (e.g., using MUSE, Meyer et al. 2020, Fig. 5). With the proposed observations, we will detect ~2 LAEs suitable for galaxy-Lyα-spike studies per QSO sightline, allowing us to detect the cross-correlation at 8σ and to **constrain the ionizing photon escape fraction at the 2% precision**. Thus, we will finally determine whether faint galaxies dominate the reionization process.

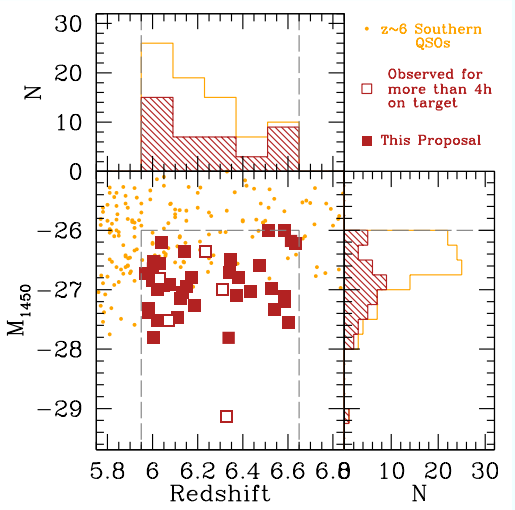

Fig. 1 – Redshifts and UV luminosities of all southern high-z QSOs known to date. Our sample consists of 40 bright $5.8<z<6.6$ QSOs. For all these objects, sensitive XSHOOTER spectra and high-resolution ALMA mm-observations have been collected (and 16 of those are target of JWST GO and GTO programs). Thus, **for all selected QSOs, the main properties of the central black holes and of the host galaxies have already been secured**. White squares mark the 5 QSOs for which >4 h MUSE integrations have already been acquired, and are thus not included in this proposal. The proposed observations target objects brighter than the characteristic magnitude of $z>6$ QSOs ($M^{*}_{1450}\sim-26.2$ mag). This will create a unique data-set to coherently investigate the close environment of $z\sim6$ QSO host galaxies (Fig. 2, 4) and to shed light on the properties of the first galaxies (Fig. 3, 5).

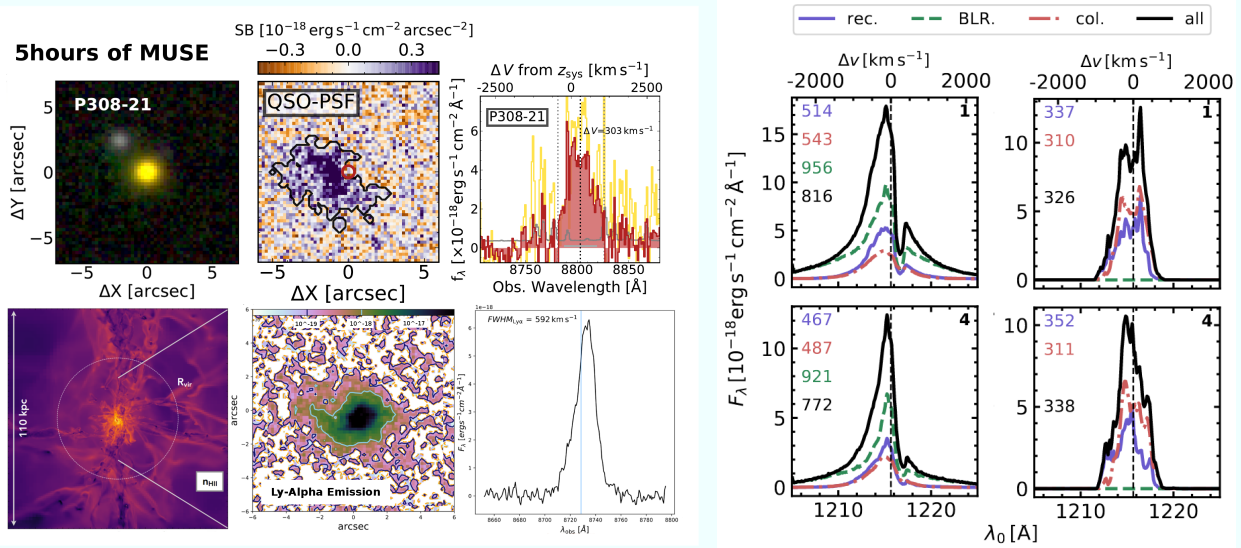

Fig. 2 – Extended Lyα halos around QSOs at z>6. *Left-Panel* – Lyα nebula detected around the z=6.23 QSO P308-21 with 5 hours of MUSE integration (Farina et al. 2019). After carefully subtracting the QSO PSF, emission (with SB(Lyα)$\sim10^{-18}$ erg s^{-1} cm^{-2} arcsec^{-1}) extending out to 40 kpc scales has been detected. Given current ALMA constraints on the SFR (10-300 $M_\odot$ yr^{-1}) and XSHOOTER measurements of the SMBH accretion rate (close to Eddington), the Lyα emission is likely due to the fluorescence of the highly ionized optically thin gas. The nebula appears to be redshifted from the host galaxy's systemic redshift (precisely traced with 0.3″ resolution ALMA observations of the [C II] emission line, Decarli et al. 2019), suggesting an ongoing inflow of gas. On the bottom, we show a radiation-hydrodynamic zoom-in simulation of a halo with $M_{Halo}=3\times10^{12}M_\odot$ at $z=6$ (Costa et al. 2022). The Lyα emission strikingly resemble the observed one in terms of extent and spectral shape, once the effects of gas outflows, and stellar and QSO photo-ionization are taken into account. The proposed program will provide a definitive and statistical picture of how the gas is feeding the growth of the first black holes and galaxies. This will set quantitative constraints for future high resolution simulations aimed at investigating the assembly of the first massive galaxies. *Right-Panel* – Simulated line profiles of the extended Lyα emission around $z\sim6$ QSOs (Costa et al. 2022). The contribution of the different mechanism powering the Lyα emission are plotted as different colored curves (blue: recombination radiation, green: BLR scattering, red: collisional excitation). The combination of all processes is showed as a black solid line. In the left column, we show results including scattering and illustrate the impact of neglecting resonant scattering in the right column. A comparison with these synthetic models with high quality spectra of the extended emission provided by our program will allow us to decode the leading contribution to the Lyα emission.

References: Arrigoni Battaia+19, MNRAS, 482, 3162 • Becker+19, ApJ, 883, 163 • Bosman+22, MNRAS, 514, 55 • Costa+22, MNRAS, 517, 1767 • Curti+23, MNRAS, 518 • Davies+18, ApJ, 864, 142 • Davies+23a, MNRAS, 521, 314 • Davies+23b, MNRAS, 521, 289 • Decarli+12, ApJ, 756, 150 • Decarli+19, ApJ, 880, 157 • D'Odorico et al. 2022, MNRAS, 512, 2389 • Díaz+21, MNRAS, 502, 2645 • Drake+19, ApJ, 881, 131 • Eilers+22, arXiv:2212.06907 • Farina+19, ApJ, 887, 196 • Farina+22, ApJ, 941, 106. • Garcia-Vergara+17, ApJ, 848, 7G • Kannan+22, MNRAS, 511, 4005 • Meyer+20, MNRAS, 494, 1560 • Meyer+22, ApJ, 927, 14M • Naidu+20, ApJ, 892, 109 • Neeleman+21, ApJ, 911, 141N • Schindler+20, ApJ, 905, 51 • Venemans+20, ApJ, 904, 130

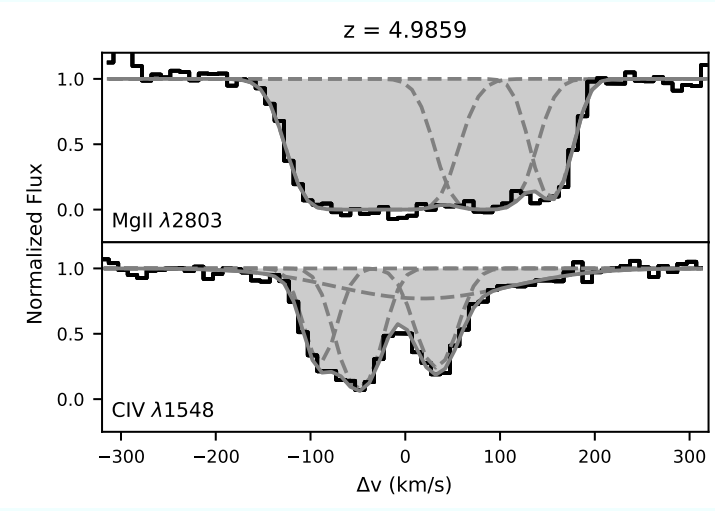

Fig. 3 – Probing the CGM-galaxy connection at high-z. Mg II + C IV absorption system detected at z=4.9859 in the XSHOOTER spectrum of the z=5.98 QSO PSO J029-29 (part of this proposal). The different components are highlighted with dashed gray lines. This system spans more than 200 km s^{-1} in velocity and shows a complex multiphase ionization and kinematic structure. Such a structure is expected to be originated by galactic winds, generated by star formation episodes, able to enrich the CGM on scales of 100 kpc (Schroetter et al. 2019). However, the interpretation of the rich wealth of information present in the absorbers relies on the MUSE driven detection of the galaxy (or multiple galaxies) where the metals first originate (Lofthouse et al. 2020).

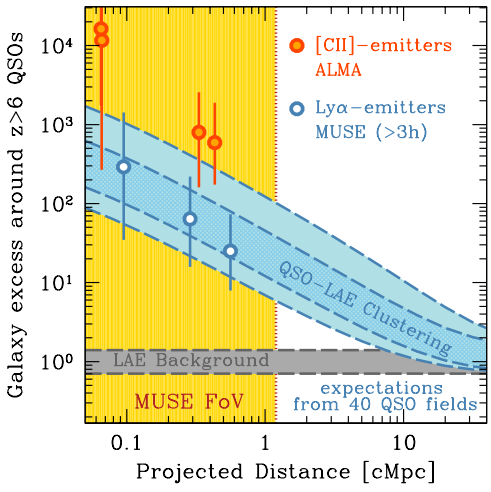

Fig. 4 – The rich environment of the first QSOs. Expected excess of LAEs in 40 QSO fields assuming the z∼6 luminosity function by Santos et al. (2016, gray shaded curve) and the QSO-galaxy two-point correlation function by Garcia-Vergara et al. (2017), calibrated at z∼4 (blue shaded curve). The width of the shaded areas (1 and 2σ uncertainties) reflects both cosmic variance and uncertainties in the luminosity function estimates. If the galaxies around z>6 QSOs are clustered as at z∼4, we expect to be able to detect ∼20-30 LAEs associated with the QSOs while 1-2 are expected in the blank field. With our sample we will be able to **quantify the small scale QSO-galaxy correlation function at z>6**. We over-plot the 3 LAEs detected in >3h deep MUSE observations of z=6-6.5 QSOs (Farina et al. 2017, Meyer et al. 2022, blue circles) and the [C II] bright companion galaxies revealed by ALMA around ∼15-30% of the explored fields (Decarli et al. 2017, with errorbars showing poissonian uncertainties only).

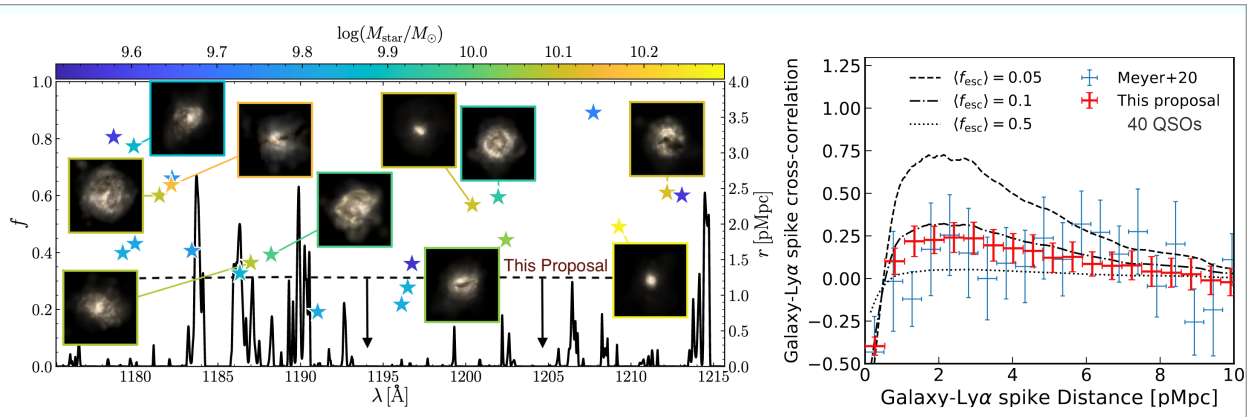

Fig. 5 – The escape fraction of z>6 galaxies. A sample of 40 QSOs observed with both MUSE and XSHOOTER is necessary to achieve the ambitious goal of a definitive measurement of the average escape fraction of z∼6 galaxies via the cross-correlation of emission spikes with LAEs (Left Panel, Garaldi et al. 2022). Different models estimate that z>6 galaxies must have an escape fraction between 10%-20% for reionization to conclude by z∼6 (e.g. Finkelstein et al. 2019, Naidu et al. 2020). By comparison, Steidel et al. (2018) report an escape fraction of 0.09±0.01 for galaxies at z<3. To distinguish between different reionization models, and to find evidence for an evolution in the properties of early galaxies, an escape fraction measurement with an absolute error $\lesssim$2% is necessary (Kakiichi et al. 2018). Current measurements of the galaxy-IGM cross-correlation have an error of ∼10% (Meyer et al. 2020, using MUSE, right Panel blue crosses) from a signal detected at 3.3σ from 8 QSO fields. We simulated the galaxy-IGM cross-correlation for the sample proposed here (Left Panel red crosses) assuming that 2 LAEs suitable for the cross-correlation will be detected per 4h MUSE datacube. We find that with 40 QSOs at z>5.8, the galaxy IGM cross-correlation will be detected at 8σ with the targeted 2% absolute error on the escape fraction (right panel red-curve).

TARGETS

Name	RA	Dec	Coord	Runs	Comment
P007P04	00:28:06.56	+04:57:25.68	J2000	2	z=6.0015,M1450=-26.6mag
JAB=20.2					
P009M10	00:38:56.52	-10:25:53.90	J2000	2	z=6.0040,M1450=-26.5mag
JAB=19.9					
J0142M3327	01:42:43.72	-33:27:45.47	J2000	1	z=6.3373,M1450=-27.8mag
JAB=18.9					
J0148P0600	01:48:37.63	+06:00:20.09	J2000	1	z=5.9800,M1450=-27.4mag
JAB=19.1					
P029M29	01:58:04.14	-29:05:19.25	J2000	1	z=5.9840,M1450=-27.3mag
JAB=19.1					
J0159M3633	01:59:57.97	-36:33:56.62	J2000	1	z=6.0200,M1450=-27.0mag
JAB=19.6					
J0224M4711	02:24:26.54	-47:11:29.40	J2000	1	z=6.5260,M1450=-27.0mag
JAB=19.7					
P036P03	02:26:01.87	+03:02:59.39	J2000	1	z=6.5405,M1450=-27.3mag
JAB=19.5					
J0305M3150	03:05:16.91	-31:50:55.90	J2000	1	z=6.6139,M1450=-26.2mag
JAB=20.6					
P056M16	03:46:52.04	-16:28:36.87	J2000	1	z=5.9670,M1450=-26.7mag
JAB=20.1					
J0408M5632	04:08:19.23	-56:32:28.80	J2000	1	z=6.0300,M1450=-26.6mag
JAB=19.9					
P065M26	04:21:38.05	-26:57:15.60	J2000	1	z=6.1871,M1450=-27.3mag
JAB=19.4					
P089M15	05:59:45.46	-15:35:00.20	J2000	1	z=6.0500,M1450=-26.9mag
JAB=19.2					
J0706P2921	07:06:26.39	+29:21:05.50	J2000	1	z=6.6037,M1450=-27.6mag
JAB=19.1					
J0818P1722	08:18:27.39	+17:22:51.79	J2000	1	z=6.0200,M1450=-27.5mag
JAB=19.5					
J0842P1218	08:42:29.42	+12:18:50.50	J2000	1	z=6.0763,M1450=-26.9mag
JAB=19.8					
J0923P0402	09:23:47.12	+04:02:54.40	J2000	1	z=6.6330,M1450=-26.2mag
JAB=20.3					
P159M02	10:36:54.19	-02:32:37.94	J2000	1	z=6.3809,M1450=-26.8mag
JAB=20.1					
P164P29	10:58:07.72	+29:30:41.70	J2000	1	z=6.5846,M1450=-26.0mag
JAB=21.2					
P167M13	11:10:33.97	-13:29:45.60	J2000	1	z=6.5144,M1450=-26.0mag
JAB=21.2					
J1148P0702	11:48:03.28	+07:02:08.33	J2000	1	z=6.3440,M1450=-26.5mag
JAB=20.2					
P183P05	12:12:26.98	+05:05:33.49	J2000	2	z=6.4330,M1450=-27.0mag
JAB=19.8					
J1319P0950	13:19:11.30	+09:50:51.49	J2000	2	z=6.1347,M1450=-27.1mag

Name	RA	Dec	Coord	Runs	Comment
JAB=19.7					
P217M16	14:28:21.39	-16:02:43.29	J2000	2	z=6.1498,M1450=-26.9mag
JAB=19.7					
P217M07	14:31:40.45	-07:24:43.30	J2000	2	z=6.1400,M1450=-26.4mag
JAB=19.9					
J1509M1749	15:09:41.77	-17:49:26.80	J2000	2	z=6.1225,M1450=-27.1mag
JAB=19.8					
P231M20	15:26:37.84	-20:50:00.66	J2000	2	z=6.5869,M1450=-27.2mag
JAB=19.6					
J1535P1943	15:35:32.87	+19:43:20.10	J2000	2	z=6.3700,M1450=-27.1mag
JAB=19.6					
P239M07	15:58:50.98	-07:24:09.59	J2000	2	z=6.1102,M1450=-27.5mag
JAB=19.4					
P247P24	16:29:11.29	+24:07:39.74	J2000	2	z=6.4760,M1450=-26.6mag
JAB=20.2					
J2054M0005	20:54:06.48	-00:05:14.80	J2000	2	z=6.0389,M1450=-26.2mag
JAB=20.1					
P323P12	21:32:33.19	+12:17:55.26	J2000	2	z=6.5872,M1450=-27.1mag
JAB=19.7					
J2211M3206	22:11:12.39	-32:06:12.94	J2000	2	z=6.3394,M1450=-26.7mag
JAB=19.5					
J2250M5015	22:50:02.01	-50:15:42.20	J2000	2	z=6.0000,M1450=-26.9mag
JAB=19.2					
J2310P1855	23:10:38.88	+18:55:19.70	J2000	2	z=6.0031,M1450=-27.8mag
JAB=18.9					
P359M06	23:56:32.45	-06:22:59.26	J2000	2	z=6.1722,M1450=-26.8mag
JAB=19.9					

Target Notes

The proposed sample is based on the recent 5-fold increase on the number of z>5.7 QSOs known in the south. We selected all the 40 bright QSOs at 5.8≤z≤6.6 located in the southern emisphere (Dec<30) for which deep XSHOOTER and ALMA observations has been already secured. This, de facto, luminosity limited sample (-29.5mag<M1450<-26mag) will allow us to perform an unbiased study of the variety of the QSO population in the crucial age of the Epoch of Reionization (see Fig. 1).

This program will unleash the full potential of current extensive ESO campaigns aimed at fully characterizing z~6 QSOs and their environment. Indeed, for ALL selected targets, high quality ALMA observations are probing the cold dust and the star forming medium of the host galaxies (Decarli et al. 2017, 2018, Venemans et al. 2016, 2017, 2018, 2020, Neeleman et al. 2019, 2021), while deep XSHOOTER optical/NIR spectra (both archival and from the 248h ESO LP “XQR-30: the ultimate XSHOOTER legacy survey of quasars at z=5.8−6.6”, Prog. ID: 1103.A-0817, PI: D'Odorico) are providing crucial information on black hole masses and accretion rates (Farina et al. 2022), on intervening metal absorbers (Becker et al. 2019, D'Odorico et al. 2022, Davies et al. 2023), and on the status of the IGM at the end of the reionization epoch (Bosman et al. 2022). Observations of the rest-frame optical luminosity and color of the host galaxies have been secured with Spitzer (Mazzucchelli et al. 2019) and their radio properties have been explored with JVLA (Bañados et al. 2018, 2021, Bosman et al. 2021). In addition, 16 of the quasars selected in this proposal are target of different JWST GTO and Cycle 1 programs. In particular, we comprise all QSOs accesible from the south part of the ASPIRE program (ID. #2078) and of the GTO program ID. #1243. The goal of these JWST observations is to detect Hβ and [OIII] line emitters in the proximity of z~6-7 QSOs. The proposed MUSE observations will provide the crucial information on the Lyα emission, allowing a truly comprehensive view of the assembly of the first QSOs.

Exposure time and sample size has been tailored to optimize the detection of LAEs at 4.0<z<6.6. This statistical sample of high-redshift galaxies will be used to investigate the cross correlation between LAEs and transmission spikes in the Lyα forest (Fig. 5) and metal absorbers (Fig. 3), and to set quantitative constraints on the clustering of galaxies around z~6 QSOs (Fig. 4).

REMARKS & JUSTIFICATIONS

Lunar Phase and Constraints Justification

Please justify here the requested lunar phase and other observing constraints.

The Lyα emission of a z>6 QSO is redshifted at λ>850nm the moon has little effect on the data quality for the QSO-galaxy clustering and for the Lyα halos science cases. However, in bright time, the data quality rapidly decreases at shorter wavelengths, impeding the efficient detection z~4.5-5.5

Lyα-emitters. The requested FLI=0.7 allow us to reach the same sensitivity for the detection of a LAEs at z=5 a factor 1.7x faster than if we would consider FLI=0.9.

Time Justification

Please describe here a detailed computation of the necessary time to execute the observations, including time-critical aspects if any. Parameters used in the ETC should be mentioned so the computation can be reproduced.

This program aims to perform a systematic study of the ecosystems of high redshift QSOs and galaxies. The exposure time is tailored to detect with high-significance (1) companion galaxies located at the precise [CII] redshift of the QSO host galaxies inferred from sensitive ALMA observations, (2) foreground LAEs associated to intervening metal absorbers and to Lyα transmission spikes detected in deep XSHOOTER spectra, (3) extended Lyα nebulae powered by UV photons rising both from the star formation activity of the host (derived from ALMA maps of the dust continuum emission) and from accretion on the central BH (directly measured from the rest-frame UV spectroscopy collected with XSHOOTER).
We base our estimates on the MUSE Exposure Time Calculator (Version P112) assuming a QSO at z~6.2 observed with 0.7 FLI with seeing=1.3" (Turbulence category=85%) and airmass=1.5. We will consider an exposure time of 4 hours per target (5 hours including overheads).

(1) Expected number of companion galaxies to a QSO:
With the propose exposure time, we will be able to probe at S/N>5 a line with F(Lyα)=2x10^-17 erg/s/cm^2 and FWHM=500km/s (binning over 5x5 spatial and 5 spectral pixels). This corresponds to L(Lyα)=8.6x10^42 erg/s, i.e. 2x fainter than the knee of the z~6 LAE luminosity function (LF, Konno et al. 2018). This lead to a volume density of n=2.0x10^-4/cMpc^3. In presence of clustering, the expected number of LAEs is boosted by a factor [1+ξ(r)], where ξ(r)=(r/r_0)^-γ is the correlation function. The volume explored extends over 20cMpc along the line of sight (the typical distance used in clustering studies) and over the 1'x1' MUSE field of view. Assuming the QSO-LAE correlation function at z~4 from Garcia-Vergara et al. (2017, with r_0=8.8cMpc and γ=2.0), we thus expect to detect 0.5 LAEs per field (at the QSO systemic redshift). Thus, one expects a total of ~20 LAEs associated with the full sample of 40 QSOs. This represents a 5σ excess over the average ~1-2 galaxies present on the blank field (i.e. in the absence of any clustering around the biased QSO hosts, Fig. 4).

(2) Expected number of foreground LAEs:
With the proposed observations we will detect at high significance (>5σ) LAEs with L(Lyα)~5.5x10^42 erg/s at z=5.5. At this depth, within a survey volume of ~10^5 cMpc^−3 between z~4.5-6.2 (i.e. in foreground respect to the QSO redshift) along 40 fields, we will discover ~80 LAEs for which we will probe the CGM in absorption. This number is consistent with the current constraint on the number density of MgII absorbers (one the most commonly used tracer of metals at high redshift) at z~5.5 (e.g., Chen et al. 2017) and with the number of strong absorbers detected in the XSHOOTER spectra of the QSOs (Fig. 3). In addition, MUSE will also reveal LAEs down to z~3. We will leverage on this dense spectroscopic survey to undertake a systematic analysis of ions inside the CGM as a function of redshift, providing a critical test for models of galaxy evolution.

(3) Extended Lyα emission:
At the proposed sensitivity, we achieve a 5σ Lyα surface brightness limit of 1x10^−18erg/s/cm^2/arcsec^2 over a 1 arcsec^2 aperture. In this regime, we will be able to compensate for the (1+z)^-4 redshift dimming factor of the surface brightness and thus to characterize Lyα emission surrounding the first QSOs at a level comparable to lower redshift studies (e.g., Arrigoni-Battaia et al. 2019). This is a fundamental step to understand which are the drivers of the observed evolutionary trend on the amount of cool gas surrounding QSOs from z~6 to z~2 (Farina et al. 2019, Fossati et al. 2021, Costa et al. 2022, Fig. 2).

In summary, including overheads (preset, acquisition, offset, and rotation) and considering data already in the archive we request 147 hours of MUSE to investigate the field of 40 z~6 QSOs (5 of which already have deep integrations).

Telescope Justification

Please justify why the telescope requested is the best choice for this programme.

The sensitivity requested in this project is only achievable with an 8m-class telescope. The IFU capabilities offered by MUSE are ideal for our goals. Being the most efficient spectrograph on the VLT with a 1'x1' FoV (corresponding to 2.4x2.4 cMpc^2 at z~6), MUSE will allow us to search for Lyα emitting galaxies in the light cone of z~6 QSOs in only 5h per source (including overheads). This represents a revolutionary step in characterizing the close environment of the first QSOs and galaxies, moving from an "exploratory regime" based on single sources to a precision regime with the investigation of a large and unbiased sample.

In addition, MUSE is the only instrument able to reach the sensitivity limit necessary to fully characterize Lyα nebular emission down to a level comparable to their z~2-3 counterparts.

Mode Justification

Please explain the choice of SM, VM or dVM.

Given the wide large of RA spanned by our targets service mode is preferred.

Calibration Request

If you need any special calibration not included in the instrument calibration plan, please specify it here.

N/A

Data Product Delivery Plan

For Large Programmes, teams are expected to deliver data products to the ESO archive (Phase 3). Please describe the team's plan to derive and release these data products (within two years of the observations).

Our team has all the expertise and resources needed to handle the data from this programme.

The primary reduction of data will be completed at MPIA, MPA, GEMINI, and INAF/Bologna, where we have access to dedicated reduction machines. The data reduction will be performed by Farina and Arrigoni-Battaia. Due to the time sensitive nature of this programme (and particularly

the legacy value for future E-ELT and JWST surveys), we plan two data-releases (roughly one per semester). In addition, we will release data reduced with ESO pipelines to the community via a collaboration website within 6 months of the date of last observations of a complete dataset for a QSO (i.e. when all the OBs for a field will be collected). Both data reduced with ESO pipelines and advanced data products (reduced with proprietary codes) will be released within 6 months of the completion of all the observations via ESO archive. The PI was part of the ESO Archive Science Group and is thus in a privileged position to ensure that these milestones will be respected.

Besides the data reduction procedure, our team has developed throughout the years a specialized library of analysis code, with which we will promptly extract galaxy catalogues from MUSE data, to start working on science results within weeks from the date of observations. The advanced data products (line lists, galaxy catalogues, 3D morpho-kinematics models) will also be made publicly available within 1 year of the end of the programme. The legacy value of this dataset, and particularly the timely delivery of reduced data products, will extend well beyond the goals of this programme, enabling the ESO community to develop strong science programmes for exploitation with JWST (Co-I Wang is the PI of the JWST Cycle 1 proposal, ID. #2078) and, in the future, with the EELT.

Our team has also sufficient resources of personnel (including several postdoctoral researchers) to complete the proposed science investigation.

Duplication with ESO Science Archive

If observations of the same target(s) using the same instrument(s) already exist in the ESO archive, please justify why this programme requests further observations.

Of the 40 target proposed here, 5 QSOs has been observed with MUSE with exposures larger than 4 hours and 23 with shallower exposures (~1-3hours). The time requested has been reduced accordingly to the data present in the archive in order to obtain an homogeneous survey depth over each field.

Duplication Justification

If an instrument GTO team aims at the same target(s), please justify why this programme requests further observations.

N/A

Background and Experience

Short description of the background, expertise and roles of the various team members in the context of the science case discussed in the proposal. For small teams the applicants may wish to provide a sentence for the qualifications of each member, while for larger teams (e.g. in Large Programmes), only the leading roles need to be specified.

The world-wide community of scientists working on the EoR using quasar spectra decided to join forces in this Large Programme to produce a legacy sample that can, for the first time, address most of the open questions in this field. Our team has comprehensive knowledge in the analysis and interpretation of QSO multi-wavelength data, covering most of the topics of this research field: from the fluctuation of the Lyman-α optical depth (Dr. Bosman, Dr. Garaldi, Dr. Meyer), to the distribution and abundances of high-redshift metals (Dr. Davies, Dr. D'Odorico, Prof. Ryan-Weber), to the properties of high-z QSOs (Dr. Neeleman, Dr. Walter).

The team is leading an extensive observing campaign to discover and fully characterize the properties of the first QSOs (with different facilities including ALMA, VLT, HST, JWST, SPITZER, and KECK) and published more than 100 papers on the topic of high redshift QSOs in the last decade. The proposed project builds on a team effort to discover the first QSOs emerging from the Cosmic Dark ages. This provided the community with more that 200 QSOs at z~6 and all the z>7.5 QSOs known to date (Dr. Banados, Prof. Fan, Dr. Mazzucchelli, Dr. Venemans, Dr. Yang, and Dr. Wang) and capitalizes on world experts on theoretical modeling and numerical simulation of early structure formation (Dr. Costa, Dr. Davies, Dr. Eilers, Dr. Garaldi, Dr. Gutcke, Prof. Hennawi, Dr. Mesinger, and Dr. Meyer).

The sample built on our effort to exploit the unparalleled capabilities of ALMA to investigate the cold dust and the star forming medium of the host galaxies in an unbiased sample of ~50 QSOs at z>6 (Dr. Walter, Dr. Decarli, Dr. Venemans, and Dr. Neeleman) and to use deep XSHOOTER spectra to investigate the crucial information on the black-hole masses, accretion rate, and metal enrichment of the QSOs as well as foreground metal absorbers (Dr. Schindler, Dr. Becker, and Prof. Ryan-Weber). In particular in Period~103 the team has been awarded the 248h XSHOOTER large program (“XQR-30: the ultimate XSHOOTER legacy survey of quasars at z=5.8−6.6”, Prog. ID: 1103.A-0817, PI: D'Odorico). The team also already employed VLT/MUSE to perform the first census of the extended Ly-Alpha emission around QSOs at 6.0<z<6.6 (Dr. Farina, Dr. Drake, and Dr. Arrigoni-Battaia) and is involved in several JWST follow up projects (Eilers et al. 2022), including the JWST GO program #2078.

REPORT ON PREVIOUS USAGE OF ESO FACILITIES

Run	PI	Instrument	Time	Mode	Comment
098.B-0537(A)	Emanuele Paolo Farina	XSHOOTER	40.0h	Service	Published in Schindler et al. 2020
The Properties of the First QSOs: new Insights from X-SHOOTER and ALMA					
0101.A-0656(A)	Emanuele Paolo Farina	MUSE	23.0h	Service	Published in Farina et al. 2019
The Ecosystem of the First QSOs -- A MUSE Snapshot Survey					
0103.A-0562(A)	Emanuele Paolo Farina	MUSE	12.0h	Service	Published in Farina et al. 2019
The Ecosystem of the First QSOs -- A MUSE Snapshot Survey					
0104.A-0948(A)	Emanuele Paolo Farina	MUSE	31.0h	Service	Data reduced, a paper is in preparation
The Ecosystem of the First QSOs -- A MUSE Snapshot Survey					
0104.A-0948(B)	Emanuele Paolo Farina	MUSE	24.0h	Service	No data collected.
The Ecosystem of the First QSOs -- A MUSE Snapshot Survey					
0100.A-0045(A)	Fabrizio Arrigoni Battaia	MUSE	17.0h	Service	Data published in Arrigoni-Battaia et al. 2019.

Run	PI	Instrument	Time	Mode	Comment
Are Giant $zsim 2 -3$ Lyman Alpha Nebulae Signposts for Overdensities of Galaxies and AGN?					
0103.A-0306(A)	Fabrizio Arrigoni Battaia	SEPIA	84.0h	Service	Data published in Munoz-Melgueta et al. 2022.
QSO MUSEUM meets APEX: unveiling the link between halo gas and molecular reservoirs of $zsim3$ QSOs					
1103.A-0817(A)	Valentina D'Odorico	XSHOOTER	112.5h	Service	Data collection recently completed. Several paper published and in preparation.
XQR-30: the ultimate XSHOOTER legacy survey of quasars at $zsimeq5.8-6.6$					
1103.A-0817(B)	Valentina D'Odorico	XSHOOTER	135.5h	Service	Data collection recently completed. Several paper published and in preparation.
XQR-30: the ultimate XSHOOTER legacy survey of quasars at $zsimeq5.8-6.6$					
0101.B-0272(A)	Anna-Christina Eilers	XSHOOTER	2.0n	Visitor	Data published in Eilers et al. 2020, 2021.
Young Quasars in the Early Universe					
2102.A-5042(A)	Chiara Mazzucchelli	XSHOOTER	4.5h	Service	Data published in Banados et al. 2021.
The central properties of the most distant radio source known at $z\sim 7$					
0103.A-0423(A)	Feige Wang	XSHOOTER	29.5h	Service	Published in Yang et al. 2020, 2021
Exploring the Cosmic Reionization and Black Hole Growth with Three New Luminous Quasars at $zsim7$.					
110.23UC.005	Chiara Mazzucchelli	FORS2	15.8h	Service	Data under acquisition
An All-Time Filler for UT1					
110.23UC.008	Chiara Mazzucchelli	FORS2	20.0h	Service	Data under acquisition
An All-Time Filler for UT1					
110.23UC.001	Chiara Mazzucchelli	FORS2	11.0h	Service	Data under acquisition
An All-Time Filler for UT1					
110.23UC.003	Chiara Mazzucchelli	FORS2	6.8h	Service	Data under acquisition
An All-Time Filler for UT1					
110.23UC.007	Chiara Mazzucchelli	FORS2	12.9h	Service	Data under acquisition
An All-Time Filler for UT1					
110.23UC.006	Chiara Mazzucchelli	FORS2	11.0h	Service	Data under acquisition
An All-Time Filler for UT1					
110.23UC.002	Chiara Mazzucchelli	FORS2	6.0h	Service	Data under acquisition
An All-Time Filler for UT1					
110.23UC.004	Chiara Mazzucchelli	FORS2	12.0h	Service	Data under acquisition
An All-Time Filler for UT1					
111.24H9.001	Chiara Mazzucchelli	FORS2	17.0h	Service	Data to be acquired in P111
The Large-Scale Environment of a Powerful Radio Loud Quasar in the Epoch of Reionization					
111.2547.001	Emanuele Paolo Farina	MUSE	4.0h	Service	Observations to be collected in P111
Shedding Light on Early Structure Formation: MUSE Unveils the Largest Ly? Nebulae around a z~6.6 QSO					

RECENT PI/CoIs PUBLICATIONS MOST RELEVANT TO THE SUBJECT OF THIS PROPOSAL

1. Bañados, E., Mazzucchelli, C., Momjian, E., et al. (2021) "The Discovery of a Highly Accreting, Radio-loud Quasar at z = 6.82," ApJ, 909, 80 - 2021ApJ...909...80B
2. Bischetti, M., Feruglio, C., D'Odorico, V., et al. (2022) "Suppression of black-hole growth by strong outflows at redshifts 5.8-6.6," Natur, 605, 244-247 - 2022Natur.605..244B
3. Bosman, S. E. I., Davies, F. B., Becker, G. D., et al. (2022) "Hydrogen reionization ends by z = 5.3: Lyman-α optical depth measured by the XQR-30 sample," MNRAS, 514, 55-76 - 2022MNRAS.514...55B
4. Costa, T., Arrigoni Battaia, F., Farina, E. P., et al. (2022) "AGN-driven outflows and the formation of Lyα nebulae around high-z quasars," MNRAS, 517, 1767-1790 - 2022MNRAS.517.1767C
5. Davies, R. L., Ryan-Weber, E., D'Odorico, V., et al. (2023) "The XQR-30 metal absorber catalogue: 778 absorption systems spanning 2 □ z □ 6.5," MNRAS, 521, 289-313 - 2023MNRAS.521..289D

6. Davies, R. L., Ryan-Weber, E., D'Odorico, V., et al. (2023) "Examining the decline in the C IV content of the Universe over 4.3 □ z □ 6.3 using the E-XQR-30 sample," MNRAS, 521, 314-331 - 2023MNRAS.521..314D

7. Díaz, C. G., Ryan-Weber, E. V., Karman, W., et al. (2021) "Faint LAEs near z > 4.7 C IV absorbers revealed by MUSE," MNRAS, 502, 2645-2663 - 2021MNRAS.502.2645D

8. D'Odorico, V., Finlator, K., Cristiani, S., et al. (2022) "The evolution of the Si IV content in the Universe from the epoch of reionization to cosmic noon," MNRAS.tmp, - 2022MNRAS.tmp..531D

9. Eilers, A.-C., Hennawi, J. F., Davies, F. B., et al. (2021) "Detecting and Characterizing Young Quasars. II. Four Quasars at z 6 with Lifetimes < 10⁴ Yr," ApJ, 917, 38 - 2021ApJ...917...38E

10. Eilers, A.-C., Simcoe, R. A., Yue, M., et al. (2022) "EIGER III. JWST/NIRCam observations of the ultra-luminous high-redshift quasar J0100+2802," arXiv, arXiv:2211.16261 - 2022arXiv221116261E

11. Farina, E. P., Schindler, J.-T., Walter, F., et al. (2022) "The X-shooter/ALMA Sample of Quasars in the Epoch of Reionization. II. Black Hole Masses, Eddington Ratios, and the Formation of the First Quasars," ApJ, 941, 106 - 2022ApJ...941..106F

12. Garaldi, E., Kannan, R., Smith, A., et al. (2022) "The THESAN project: properties of the intergalactic medium and its connection to reionization-era galaxies," MNRAS.tmp, - 2022MNRAS.tmp..401G

13. Hennawi, J. F., Davies, F. B., Wang, F., et al. (2021) "Probing reionization and early cosmic enrichment with the Mg II forest," MNRAS, 506, 2963-2984 - 2021MNRAS.506.2963H

14. Neeleman, M., Novak, M., Venemans, B. P., et al. (2021) "The Kinematics of z □ 6 Quasar Host Galaxies," ApJ, 911, 141 - 2021ApJ...911..141N

15. Schindler, J.-T., Farina, E. P., Bañados, E., et al. (2020) "The X-SHOOTER/ALMA Sample of Quasars in the Epoch of Reionization. I. NIR Spectral Modeling, Iron Enrichment, and Broad Emission Line Properties," ApJ, 905, 51 - 2020ApJ...905...51S

16. Venemans, B. P., Walter, F., Neeleman, M., et al. (2020) "Kiloparsec-scale ALMA Imaging of [C II] and Dust Continuum Emission of 27 Quasar Host Galaxies at z □ 6," ApJ, 904, 130 - 2020ApJ...904..130V

17. Walter, F., Neeleman, M., Decarli, R., et al. (2022) "ALMA 200 pc Imaging of a z 7 Quasar Reveals a Compact, Disk-like Host Galaxy," ApJ, 927, 21 - 2022ApJ...927...21W

18. Wang, F., Fan, X., Yang, J., et al. (2021) "Revealing the Accretion Physics of Supermassive Black Holes at Redshift z □ 7 with Chandra and Infrared Observations," ApJ, 908, 53 - 2021ApJ...908...53W

19. Wang, F., Yang, J., Fan, X., et al. (2021) "A Luminous Quasar at Redshift 7.642," ApJL, 907, L1 - 2021ApJ...907L...1W

20. Yang, J., Wang, F., Fan, X., et al. (2021) "Probing Early Supermassive Black Hole Growth and Quasar Evolution with Near-infrared Spectroscopy of 37 Reionization-era Quasars at 6.3 < z ≤ 7.64," ApJ, 923, 262 - 2021ApJ...923..262Y

INVESTIGATORS

Emanuele Paolo Farina, Gemini Observatory - NOIRLab, United States (PI)
Fabrizio Arrigoni Battaia, Max-Planck-Institut für Astrophysik - Garching, Germany
Eduardo Banados, Max-Planck-Institut für Astronomie - Heidelberg, Germany
George Becker, University of California - Riverside, United States
Fuyan Bian, ESO Chile, ESO
Manuela Bischetti, Universita di Trieste, Italy
Sarah Bosman, Max-Planck-Institut für Astronomie - Heidelberg, Germany
Stefano Carniani, Scuola Normale Superiore di Pisa, Italy
Thomas Connor, Harvard-Smithsonian Center for Astrophysics, United States
Tiago Costa, Max-Planck-Institut für Astrophysik - Garching, Germany
Frederick Davies, Max-Planck-Institut für Astronomie - Heidelberg, Germany
Roberto Decarli, INAF - Osservatorio di astrofisica e scienza dello spazio di Bologna, Italy
Valentina D'Odorico, INAF - Osservatorio Astronomico di Trieste, Italy
Rebecca Davies, Swinburne University of Technology, Australia
Alyssa Drake, Max-Planck-Institut für Astronomie - Heidelberg, Germany
Anna-Christina Eilers, Massachusetts Institute of Technology, United States
Xiaohui Fan, University of Arizona, United States
Andrea Ferrara, Scuola Normale Superiore di Pisa, Italy
Chiara Feruglio, INAF - Osservatorio Astronomico di Trieste, Italy
Prakash Gaikwad, Max-Planck-Institut für Astronomie - Heidelberg, Germany
Simona Gallerani, Scuola Normale Superiore di Pisa, Italy
Enrico Garaldi, Max-Planck-Institut für Astrophysik - Garching, Germany

Thales Gutcke, Max-Planck-Institut für Astrophysik - Garching, Germany
Joseph Hennawi, Leiden University, The Netherlands
Laura Keating, University of Edinburgh, United Kingdom
Yana Khusanova, Max-Planck-Institut für Astronomie - Heidelberg, Germany
Girish Kulkarni, Tata Institute of Fundamental Research - Mumbai, India
Mingyu Li, Tsinghua University - Beijing, China
Xiaojing Lin, Tsinghua University - Beijing, China
Chiara Mazzucchelli, Universidad Diego Portales, Chile
Andrei Mesinger, Scuola Normale Superiore di Pisa, Italy
Romain Meyer, Max-Planck-Institut für Astronomie - Heidelberg, Germany
Marcel Neeleman, Max-Planck-Institut für Astronomie - Heidelberg, Germany
Masafusa Onoue, Kavli Institute for Astronomy and Astrophysics - Peking University, China
Yuxiang Qin, University of Melbourne, Australia
Jan-Torge Schindler, Leiden University, The Netherlands
Bram Venemans, Leiden University, The Netherlands
Benny Trakhtenbrot, Tel Aviv University, Israel
Maxime Trebitsch, University of Groningen, The Netherlands
Roberta Tripodi, No institute, Italy
Fabian Walter, Max-Planck-Institut für Astronomie - Heidelberg, Germany
Feige Wang, University of Arizona, United States
Emma Ryan-Weber, Swinburne University of Technology, Australia
Yunjing Wu, Tsinghua University - Beijing, China
Jinyi Yang, University of Arizona, United States
Minghao Yue, Massachusetts Institute of Technology, United States
Yongda Zhu, University of California - Riverside, United States
Siwei Zou, Tsinghua University - Beijing, China

OBSERVATIONS

In the table below, the repeat factor is applied to the complete observation on that target, including its overhead.

✔ The PI acknowledged that all the telescope times listed below include overheads.

Run 112.262L.001 • Run 1 • P112 • MUSE • SM — Tel. Time: 81h00m

FLI: 70% • Turb.: 85% • pwv: 30.0mm • Sky: Variable, thin cirrus • Airmass: 1.5

Target • J0142M3327 • 01:42:43.72 • -33:27:45.47 — Tel. Time: 04h00m

OS 1	WFM-NOAO	Observation
Tel. Time: 3600 s	Instrument Mode: WFM-NOAO-N	Integration Time: 2960 s
Repeat: 4 x	Telescope Overheads: 360 s	Instrument Overheads: 280 s
Total Tel. Time: 04h00m		Signal/Noise: 5.0

Target • J0148P0600 • 01:48:37.63 • +06:00:20.09 — Tel. Time: 02h00m

OS 1	WFM-NOAO	Observation
Tel. Time: 3600 s	Instrument Mode: WFM-NOAO-N	Integration Time: 2960 s
Repeat: 2 x	Telescope Overheads: 360 s	Instrument Overheads: 280 s
Total Tel. Time: 7200s		Signal/Noise: 5.0

Target • P029M29 • 01:58:04.14 • -29:05:19.25 — Tel. Time: 05h00m

OS 1	WFM-NOAO	Observation
Tel. Time: 3600 s	Instrument Mode: WFM-NOAO-N	Integration Time: 2960 s
Repeat: 5 x	Telescope Overheads: 360 s	Instrument Overheads: 280 s
Total Tel. Time: 05h00m		Signal/Noise: 5.0

Target • J0159M3633 • 01:59:57.97 • -36:33:56.62 — Tel. Time: 05h00m

OS 1	WFM-NOAO	Observation
Tel. Time: 3600 s	Instrument Mode: WFM-NOAO-N	Integration Time: 2960 s
Repeat: 5 x	Telescope Overheads: 360 s	Instrument Overheads: 280 s
Total Tel. Time: 05h00m		Signal/Noise: 5.0

Target • J0224M4711 • 02:24:26.54 • -47:11:29.40 — Tel. Time: 04h00m

OS 1	WFM-NOAO	Observation
Tel. Time: 3600 s	Instrument Mode: WFM-NOAO-N	Integration Time: 2960 s
Repeat: 4 x	Telescope Overheads: 360 s	Instrument Overheads: 280 s
Total Tel. Time: 04h00m		Signal/Noise: 5.0

Target • P036P03 • 02:26:01.87 • +03:02:59.39 Tel. Time: 04h00m

OS 1	WFM-NOAO	Observation
Tel. Time: 3600 s	Instrument Mode: WFM-NOAO-N	Integration Time: 2960 s
Repeat: 4 x	Telescope Overheads: 360 s	Instrument Overheads: 280 s
Total Tel. Time: 04h00m		Signal/Noise: 5.0

Target • J0305M3150 • 03:05:16.91 • -31:50:55.90 Tel. Time: 02h00m

OS 1	WFM-NOAO	Observation
Tel. Time: 3600 s	Instrument Mode: WFM-NOAO-N	Integration Time: 2960 s
Repeat: 2 x	Telescope Overheads: 360 s	Instrument Overheads: 280 s
Total Tel. Time: 7200s		Signal/Noise: 5.0

Target • P056M16 • 03:46:52.04 • -16:28:36.87 Tel. Time: 05h00m

OS 1	WFM-NOAO	Observation
Tel. Time: 3600 s	Instrument Mode: WFM-NOAO-N	Integration Time: 2960 s
Repeat: 5 x	Telescope Overheads: 360 s	Instrument Overheads: 280 s
Total Tel. Time: 05h00m		Signal/Noise: 5.0

Target • J0408M5632 • 04:08:19.23 • -56:32:28.80 Tel. Time: 05h00m

OS 1	WFM-NOAO	Observation
Tel. Time: 3600 s	Instrument Mode: WFM-NOAO-N	Integration Time: 2960 s
Repeat: 5 x	Telescope Overheads: 360 s	Instrument Overheads: 280 s
Total Tel. Time: 05h00m		Signal/Noise: 5.0

Target • P065M26 • 04:21:38.05 • -26:57:15.60 Tel. Time: 04h00m

OS 1	WFM-NOAO	Observation
Tel. Time: 3600 s	Instrument Mode: WFM-NOAO-N	Integration Time: 2960 s
Repeat: 4 x	Telescope Overheads: 360 s	Instrument Overheads: 280 s
Total Tel. Time: 04h00m		Signal/Noise: 5.0

Target • P089M15 • 05:59:45.46 • -15:35:00.20 Tel. Time: 05h00m

OS 1	WFM-NOAO	Observation
Tel. Time: 3600 s	Instrument Mode: WFM-NOAO-N	Integration Time: 2960 s
Repeat: 5 x	Telescope Overheads: 360 s	Instrument Overheads: 280 s
Total Tel. Time: 05h00m		Signal/Noise: 5.0

Target • J0706P2921 • 07:06:26.39 • +29:21:05.50 Tel. Time: 05h00m

OS 1	WFM-NOAO	Observation
Tel. Time: 3600 s	Instrument Mode: WFM-NOAO-N	Integration Time: 2960 s
Repeat: 5 x	Telescope Overheads: 360 s	Instrument Overheads: 280 s
Total Tel. Time: 05h00m		Signal/Noise: 5.0

Target • J0818P1722 • 08:18:27.39 • +17:22:51.79 Tel. Time: 05h00m

OS 1	WFM-NOAO	Observation
Tel. Time: 3600 s	Instrument Mode: WFM-NOAO-N	Integration Time: 2960 s
Repeat: 5 x	Telescope Overheads: 360 s	Instrument Overheads: 280 s
Total Tel. Time: 05h00m		Signal/Noise: 5.0

Target • J0842P1218 • 08:42:29.42 • +12:18:50.50 Tel. Time: 04h00m

OS 1	WFM-NOAO	Observation
Tel. Time: 3600 s	Instrument Mode: WFM-NOAO-N	Integration Time: 2960 s
Repeat: 4 x	Telescope Overheads: 360 s	Instrument Overheads: 280 s
Total Tel. Time: 04h00m		Signal/Noise: 5.0

Target • J0923P0402 • 09:23:47.12 • +04:02:54.40 Tel. Time: 04h00m

OS 1	WFM-NOAO	Observation
Tel. Time: 3600 s	Instrument Mode: WFM-NOAO-N	Integration Time: 2960 s
Repeat: 4 x	Telescope Overheads: 360 s	Instrument Overheads: 280 s
Total Tel. Time: 04h00m		Signal/Noise: 5.0

Target • P159M02 • 10:36:54.19 • -02:32:37.94 Tel. Time: 05h00m

OS 1	WFM-NOAO	Observation
Tel. Time: 3600 s	Instrument Mode: WFM-NOAO-N	Integration Time: 2960 s
Repeat: 5 x	Telescope Overheads: 360 s	Instrument Overheads: 280 s

Total Tel. Time: 05h00m | Signal/Noise: 5.0

Target • P164P29 • 10:58:07.72 • +29:30:41.70 — Tel. Time: 05h00m

OS 1	WFM-NOAO	Observation
Tel. Time: 3600 s	Instrument Mode: WFM-NOAO-N	Integration Time: 2960 s
Repeat: 5 x	Telescope Overheads: 360 s	Instrument Overheads: 280 s
Total Tel. Time: 05h00m		Signal/Noise: 5.0

Target • P167M13 • 11:10:33.97 • -13:29:45.60 — Tel. Time: 03h00m

OS 1	WFM-NOAO	Observation
Tel. Time: 3600 s	Instrument Mode: WFM-NOAO-N	Integration Time: 2960 s
Repeat: 3 x	Telescope Overheads: 360 s	Instrument Overheads: 280 s
Total Tel. Time: 03h00m		Signal/Noise: 5.0

Target • J1148P0702 • 11:48:03.28 • +07:02:08.33 — Tel. Time: 05h00m

OS 1	WFM-NOAO	Observation
Tel. Time: 3600 s	Instrument Mode: WFM-NOAO-N	Integration Time: 2960 s
Repeat: 5 x	Telescope Overheads: 360 s	Instrument Overheads: 280 s
Total Tel. Time: 05h00m		Signal/Noise: 5.0

Run 112.262L.002 • Run 2 • P113 • MUSE • SM — Tel. Time: 66h00m

FLI: 70% • Turb.: 85% • pwv: 30.0mm • Sky: Variable, thin cirrus • Airmass: 1.5

Target • P007P04 • 00:28:06.56 • +04:57:25.68 — Tel. Time: 04h00m

OS 1	WFM-NOAO	Observation
Tel. Time: 3600 s	Instrument Mode: WFM-NOAO-N	Integration Time: 2960 s
Repeat: 4 x	Telescope Overheads: 360 s	Instrument Overheads: 280 s
Total Tel. Time: 04h00m		Signal/Noise: 5.0

Target • P009M10 • 00:38:56.52 • -10:25:53.90 — Tel. Time: 04h00m

OS 1	WFM-NOAO	Observation
Tel. Time: 3600 s	Instrument Mode: WFM-NOAO-N	Integration Time: 2960 s
Repeat: 4 x	Telescope Overheads: 360 s	Instrument Overheads: 280 s
Total Tel. Time: 04h00m		Signal/Noise: 5.0

Target • P183P05 • 12:12:26.98 • +05:05:33.49 — Tel. Time: 04h00m

OS 1	WFM-NOAO	Observation
Tel. Time: 3600 s	Instrument Mode: WFM-NOAO-N	Integration Time: 2960 s
Repeat: 4 x	Telescope Overheads: 360 s	Instrument Overheads: 280 s
Total Tel. Time: 04h00m		Signal/Noise: 5.0

Target • J1319P0950 • 13:19:11.30 • +09:50:51.49 — Tel. Time: 03h00m

OS 1	WFM-NOAO	Observation
Tel. Time: 3600 s	Instrument Mode: WFM-NOAO-N	Integration Time: 2960 s
Repeat: 3 x	Telescope Overheads: 360 s	Instrument Overheads: 280 s
Total Tel. Time: 03h00m		Signal/Noise: 5.0

Target • P217M16 • 14:28:21.39 • -16:02:43.29 — Tel. Time: 04h00m

OS 1	WFM-NOAO	Observation
Tel. Time: 3600 s	Instrument Mode: WFM-NOAO-N	Integration Time: 2960 s
Repeat: 4 x	Telescope Overheads: 360 s	Instrument Overheads: 280 s
Total Tel. Time: 04h00m		Signal/Noise: 5.0

Target • P217M07 • 14:31:40.45 • -07:24:43.30 — Tel. Time: 05h00m

OS 1	WFM-NOAO	Observation
Tel. Time: 3600 s	Instrument Mode: WFM-NOAO-N	Integration Time: 2960 s
Repeat: 5 x	Telescope Overheads: 360 s	Instrument Overheads: 280 s
Total Tel. Time: 05h00m		Signal/Noise: 5.0

Target • J1509M1749 • 15:09:41.77 • -17:49:26.80 — Tel. Time: 04h00m

OS 1	WFM-NOAO	Observation
Tel. Time: 3600 s	Instrument Mode: WFM-NOAO-N	Integration Time: 2960 s
Repeat: 4 x	Telescope Overheads: 360 s	Instrument Overheads: 280 s
Total Tel. Time: 04h00m		Signal/Noise: 5.0

Target • P231M20 • 15:26:37.84 • -20:50:00.66 Tel. Time: 01h00m

OS 1	WFM-NOAO	Observation
Tel. Time: 3600 s	Instrument Mode: WFM-NOAO-N	Integration Time: 2960 s
Repeat: 1 x	Telescope Overheads: 360 s	Instrument Overheads: 280 s
Total Tel. Time: 3600s		Signal/Noise: 5.0

Target • J1535P1943 • 15:35:32.87 • +19:43:20.10 Tel. Time: 04h00m

OS 1	WFM-NOAO	Observation
Tel. Time: 3600 s	Instrument Mode: WFM-NOAO-N	Integration Time: 2960 s
Repeat: 4 x	Telescope Overheads: 360 s	Instrument Overheads: 280 s
Total Tel. Time: 04h00m		Signal/Noise: 5.0

Target • P239M07 • 15:58:50.98 • -07:24:09.59 Tel. Time: 05h00m

OS 1	WFM-NOAO	Observation
Tel. Time: 3600 s	Instrument Mode: WFM-NOAO-N	Integration Time: 2960 s
Repeat: 5 x	Telescope Overheads: 360 s	Instrument Overheads: 280 s
Total Tel. Time: 05h00m		Signal/Noise: 5.0

Target • P247P24 • 16:29:11.29 • +24:07:39.74 Tel. Time: 04h00m

OS 1	WFM-NOAO	Observation
Tel. Time: 3600 s	Instrument Mode: WFM-NOAO-N	Integration Time: 2960 s
Repeat: 4 x	Telescope Overheads: 360 s	Instrument Overheads: 280 s
Total Tel. Time: 04h00m		Signal/Noise: 5.0

Target • J2054M0005 • 20:54:06.48 • -00:05:14.80 Tel. Time: 03h00m

OS 1	WFM-NOAO	Observation
Tel. Time: 3600 s	Instrument Mode: WFM-NOAO-N	Integration Time: 2960 s
Repeat: 3 x	Telescope Overheads: 360 s	Instrument Overheads: 280 s
Total Tel. Time: 03h00m		Signal/Noise: 5.0

Target • P323P12 • 21:32:33.19 • +12:17:55.26 Tel. Time: 04h00m

OS 1	WFM-NOAO	Observation
Tel. Time: 3600 s	Instrument Mode: WFM-NOAO-N	Integration Time: 2960 s
Repeat: 4 x	Telescope Overheads: 360 s	Instrument Overheads: 280 s
Total Tel. Time: 04h00m		Signal/Noise: 5.0

Target • J2211M3206 • 22:11:12.39 • -32:06:12.94 Tel. Time: 04h00m

OS 1	WFM-NOAO	Observation
Tel. Time: 3600 s	Instrument Mode: WFM-NOAO-N	Integration Time: 2960 s
Repeat: 4 x	Telescope Overheads: 360 s	Instrument Overheads: 280 s
Total Tel. Time: 04h00m		Signal/Noise: 5.0

Target • J2250M5015 • 22:50:02.01 • -50:15:42.20 Tel. Time: 05h00m

OS 1	WFM-NOAO	Observation
Tel. Time: 3600 s	Instrument Mode: WFM-NOAO-N	Integration Time: 2960 s
Repeat: 5 x	Telescope Overheads: 360 s	Instrument Overheads: 280 s
Total Tel. Time: 05h00m		Signal/Noise: 5.0

Target • J2310P1855 • 23:10:38.88 • +18:55:19.70 Tel. Time: 04h00m

OS 1	WFM-NOAO	Observation
Tel. Time: 3600 s	Instrument Mode: WFM-NOAO-N	Integration Time: 2960 s
Repeat: 4 x	Telescope Overheads: 360 s	Instrument Overheads: 280 s
Total Tel. Time: 04h00m		Signal/Noise: 5.0

Target • P359M06 • 23:56:32.45 • -06:22:59.26 Tel. Time: 04h00m

OS 1	WFM-NOAO	Observation
Tel. Time: 3600 s	Instrument Mode: WFM-NOAO-N	Integration Time: 2960 s
Repeat: 4 x	Telescope Overheads: 360 s	Instrument Overheads: 280 s
Total Tel. Time: 04h00m		Signal/Noise: 5.0